Constraining the ΛCDM and wCDM Models of the Universe using Gravitational Lensing

Yashvardhan Marda, Dron Paul Choudhury

University of California, Los Angeles (UCLA), Los Angeles, CA 90095, USA

yashvardhan27@ucla.edu dron975@ucla.edu

Abstract

We investigate late-time cosmology using a compiled sample of ≈ 85 galaxy-scale strong gravitational lenses, exploiting the fact that lensing directly probes geometry through the distance ratio D_{ls}/D_s while remaining effectively independent of the Hubble constant H_0. For each system we infer D_{ls}/D_s from the observed Einstein radius and stellar velocity dispersion under a standard, spherically symmetric mass description of the lens galaxy. We then confront these measurements with the predictions of two dark-energy scenarios in a spatially flat universe: ΛCDM (cosmological constant) and wCDM with a constant, yet free, equation-of-state parameter w. The theoretical distance ratios are computed from the expansion history $E(z)$ and line-of-sight integrals between the lens and source redshifts.

Parameter estimation proceeds via a straightforward χ^2 minimization built from per-lens uncertainties, yielding (i) profiled one-dimensional likelihood curves for Ω_{m0} and w, and (ii) joint confidence contours in the (Ω_{m0}, w) plane. The resulting constraints demonstrate that strong lensing alone provides precise, H_0-independent information on the matter density and dark-energy phenomenology. In ΛCDM, the best-fit matter density and its confidence interval are obtained from the profiled χ^2 curve; in wCDM, the two-parameter contours capture the expected degeneracy between Ω_{m0} and w while still delivering competitive bounds on each.

Overall, our analysis shows that a uniform treatment of galaxy-scale lenses—linking well-measured imaging and stellar kinematics to distance-ratio predictions—offers a clean and efficient route to cosmological constraints. The framework is simple, reproducible, and readily extensible: it can incorporate alternative lens models, larger samples, or be combined with complementary probes (e.g., supernovae, BAO, CMB) to further sharpen constraints and test the robustness of the late-time expansion.

1 Introduction

Strong gravitational lensing has progressed from a conceptual curiosity to a precision tool in cosmology. By producing multiple images, arcs, and Einstein rings, lenses turn galaxies into laboratories where mass, light, and distance meet in the same equations. Since the discovery of late–time acceleration [9, 11], a central task has been to map the expansion history well enough to distinguish a cosmological constant from more general dark–energy behaviors. Lensing contributes uniquely to this task because its key geometric quantity depends on *ratios* of angular–diameter distances and is thus effectively independent of H_0—a clean complement to standard candles and rulers [10].

This paper uses galaxy–scale lenses as a *geometric* probe of the late–time Universe and addresses two questions: (i) within flat ΛCDM, what matter density is preferred by lensing geometry alone? (ii) within flat wCDM, how tightly can a constant w be bounded, and how does it covary with Ω_{m0}? The lens–source redshift lever arm places sensitivity squarely in the late epochs most relevant for dark energy, while the direct link to enclosed mass keeps the inference physically transparent.

Contributions. (1) We assemble a uniform, lensing–only analysis pipeline that carries imaging and stellar kinematics through to cosmological *distance–ratio* constraints, emphasizing simplicity and reproducibility. (2) We report constraints on Ω_{m0} in flat ΛCDM and on (Ω_{m0}, w) in flat wCDM, presented both as concise one–parameter profiles and as joint confidence regions that make parameter degeneracies explicit. (3) We frame the results for straightforward combination with external probes (SNe Ia, BAO, CMB), positioning strong lensing as an H_0–independent cross–check on late–time dynamics.

This paper is organized as follows. In Section 2, we briefly describe the methodology. In Section 3 we introduce the strong–lensing dataset used in our analysis. Results are presented in Section 4 and conclusions in Section 5.

2 Methodology

The goal of this work is to use galaxy–scale strong lenses as a purely geometric probe of the late–time expansion in a spatially flat universe, testing both ΛCDM and its minimal extension with a constant dark–energy equation of state (wCDM). Throughout we assume a single lens plane, negligible external convergence in the baseline analysis, and a spherically symmetric mass description of the lens galaxy adequate for relating the Einstein radius to the enclosed mass. We adopt SI units, take all angles in radians, and reserve subscripts L, S, LS for lens, source, and lens–to–source distances, respectively. The notation Ω_{m0} denotes the present–day matter density parameter and $w \equiv p_{\rm DE}/\rho_{\rm DE}$ a constant equation–of–state parameter for dark energy.

Expansion history and distances. The expansion history is encoded in the dimensionless Hubble function $E(z) \equiv H(z)/H_0$. In the flat models considered here,

$$E(z) = \begin{cases} \sqrt{\Omega_{m0}(1+z)^3 + (1-\Omega_{m0})}, & \text{flat } \Lambda\text{CDM}, \\ \sqrt{\Omega_{m0}(1+z)^3 + (1-\Omega_{m0})(1+z)^{3(1+w)}}, & \text{flat } w\text{CDM (constant } w). \end{cases}$$

It is convenient to work with the (dimensionless) comoving distance

$$\chi(z) = \int_0^z \frac{dz'}{E(z')}\,, \tag{1}$$

from which the flat–FRW angular–diameter distance between two redshifts $z_1 < z_2$ follows as

$$D_A(z_1, z_2) = \frac{c}{H_0}\,\frac{\chi(z_2) - \chi(z_1)}{1+z_2}\,. \tag{2}$$

The geometry relevant for lensing enters only through the ratio D_{LS}/D_S, which eliminates the overall scale c/H_0 when formed from Eq. (3). Consequently, the theory prediction used below is effectively independent of H_0.

Lensing geometry and the observable. For a spherically symmetric lens producing an Einstein ring of angular radius θ_E, the reduced deflection at θ_E equals θ_E itself. In the Singular Isothermal Sphere (SIS) limit this yields

$$\theta_E = \frac{4\pi\,\sigma^2}{c^2}\,\frac{D_{LS}}{D_S}\,, \tag{3}$$

where σ is the line–of–sight stellar velocity dispersion of the lens galaxy measured from spectroscopy. Equation (4) provides a direct estimator of the distance ratio per lens:

$$D_{\rm obs} \equiv \left(\frac{D_{LS}}{D_S}\right)_{\rm obs} = \frac{c^2}{4\pi}\,\frac{\theta_E}{\sigma^2}\,. \tag{4}$$

In practice θ_E is obtained from image astrometry (or lens–model fits) and σ from aperture spectroscopy of the lens galaxy. When necessary, all angles are converted to radians before use.

Lens mass model (baseline and generalization). The baseline mapping employs the SIS relation above, appropriate for massive early–type lenses near the Einstein radius. If one instead adopts a spherical power–law density profile $\rho \propto r^{-\gamma}$ and measures a luminosity–weighted dispersion $\sigma_{\rm ap}$ within an aperture $\theta_{\rm ap}$, the inferred ratio becomes

$$\left(\frac{D_{LS}}{D_S}\right)_{\rm obs} = \frac{c^2\,\theta_E}{4\pi\,\sigma_{\rm ap}^2}\left(\frac{\theta_{\rm ap}}{\theta_E}\right)^{2-\gamma}\frac{1}{f(\gamma)}\,,$$

where $f(\gamma)$ is the standard isotropic Jeans factor,

$$f(\gamma) = -\frac{1}{(5-2\gamma)(1-\gamma)}\,\frac{\sqrt{\pi}\,\Gamma\!\left(\frac{\gamma}{2}-\frac{1}{2}\right)}{\Gamma\!\left(\frac{\gamma}{2}\right)}\,\frac{\Gamma(\gamma-1)}{\Gamma\!\left(\gamma-\frac{3}{2}\right)}\,.$$

Our cosmological analysis uses the SIS baseline for simplicity and uniformity; the pipeline can substitute the power–law expression without altering the cosmology integrals or the χ^2 construction presented below.

Data contents and selection. Each lens in the catalog contributes the tuple $\{z_l, z_s, \theta_E, \sigma\}$ with corresponding 1σ uncertainties $\{\sigma_{z_l}, \sigma_{z_s}, \sigma_\theta, \sigma_\sigma\}$. We retain only systems with $z_s > z_l$, finite positive uncertainties, and well–resolved Einstein radii. If multiple measurements exist for the same system, a deterministic priority order is adopted (e.g., most recent reduction; validated instrument pipeline), otherwise measurements are averaged inverse–variance–weighted. Where no explicit σ_θ is reported, a conservative fractional uncertainty is adopted (a fixed percentage consistent with survey systematics), clearly documented in the data table.

Uncertainty propagation for the observable. Assuming uncorrelated errors in θ_E and σ, the fractional uncertainty in Eq. (5) is

$$\left(\frac{\sigma_D}{D_{\rm obs}}\right)^2 = \left(\frac{\sigma_\theta}{\theta_E}\right)^2 + 4\left(\frac{\sigma_\sigma}{\sigma}\right)^2 , \tag{5}$$

applied lens–by–lens to obtain $\sigma_{D,i}$ for use in the likelihood below. (If a dispersion rescale is used, propagate the quoted uncertainty.)

Theory prediction per lens. Given (z_l, z_s) for a lens, the theoretical counterpart of Eq. (5) is

$$D_{\rm th}(z_l, z_s; \Theta) \equiv \frac{D_{LS}}{D_S} = \frac{D_A(z_l, z_s)}{D_A(0, z_s)} = \frac{\displaystyle\int_{z_l}^{z_s} \frac{dz'}{E(z';\Theta)}}{\displaystyle\int_0^{z_s} \frac{dz'}{E(z';\Theta)}} , \tag{6}$$

where the parameter set is $\Theta = \{\Omega_{m0}\}$ for flat ΛCDM and $\Theta = \{\Omega_{m0}, w\}$ for flat wCDM, and $E(z';\Theta)$ is given by Eq. (1). The numerator and denominator are evaluated numerically to a fixed tolerance, and the result is checked to satisfy $0 < D_{\rm th} < 1$ for all valid redshift pairs.

Numerical evaluation and caching. To ensure efficiency and reproducibility, the redshift grid used in the integrals is constructed from the unique set of lens and source redshifts in the catalog (augmented by $z = 0$), and the comoving integral $\chi(z)$ in Eq. (2) is computed once per grid point using a stable quadrature rule (e.g., adaptive Gauss–Kronrod or composite Simpson with step control). The values $\chi(z)$ are cached and reused to form D_A via Eq. (3) and hence $D_{\rm th}$ via Eq. (7). All constants (c, conversion factors) are defined in a single place and unit–checked. Inputs are validated for monotonicity of redshifts ($z_s > z_l$) and for numerical pathologies (NaNs, infs), which trigger explicit, logged exclusions.

Quality control and physical sanity checks. Because $D_{LS}/D_S \leq 1$ in standard FRW cosmology with a single lens plane, systems with $D_{\rm obs} - \sigma_D > 1$ are flagged as inconsistent under the baseline assumptions. These may indicate measurement issues, complex environments, multipane lensing, or model mismatch. The baseline fit is performed on the full quality–controlled sample; a predefined alternate cut (removing flagged outliers) is used later as a robustness check. Neither branch alters the estimator defined below.

Parameter domain and evaluation strategy. Parameter exploration proceeds on a dense, rectangular grid covering physically motivated ranges sufficient to bracket the posterior support, for example

$$\Omega_{m0} \in [\Omega_{m0}^{\rm min}, \Omega_{m0}^{\rm max}] , \qquad w \in [w^{\rm min}, w^{\rm max}] \quad (\text{for } w\text{CDM}) , \tag{7}$$

with step sizes chosen to resolve the curvature of $\chi^2(\Theta)$ (validated by refinement tests). At each grid point Θ the full set of $D_{\rm th}(z_{l,i}, z_{s,i}; \Theta)$ is formed and compared to the observables.

Estimator and confidence construction. The goodness–of–fit function is

$$\chi^2(\Theta) = \sum_{i=1}^{N} \frac{\left[D_{\rm th}(z_{l,i}, z_{s,i}; \Theta) - D_{{\rm obs},i}\right]^2}{\sigma_{D,i}^2} , \tag{8}$$

with degrees of freedom $\nu = N - 1$ for flat ΛCDM (one free parameter) and $\nu = N - 2$ for flat wCDM (two free parameters). The best–fit parameters $\widehat{\Theta}$ are those minimizing Eq. (9). One–parameter confidence intervals are reported from profiled curves (minimizing over the nuisance parameter, if present) using the standard thresholds $\Delta\chi^2 \equiv \chi^2 - \chi^2_{\rm min} = 1$ (68%) and 4 (95%). Joint two–parameter confidence regions in (Ω_{m0}, w) correspond to $\Delta\chi^2 = \{2.30, 6.18, 11.83\}$ for 1σ, 2σ, and 3σ. Around the minimum, a local quadratic

or spline interpolation of χ^2 is used purely for reporting smooth parameter estimates and uncertainties; all quoted values trace back to Eq. (9) evaluated on the native grid.

Reproducibility, safeguards, and audit trail. All numerical tolerances (integration accuracy, grid steps), constants, and selection criteria are fixed in a configuration file that accompanies the analysis. Intermediate arrays—$\chi(z)$, $D_A(z_1, z_2)$, $D_{\rm th}$, $D_{\rm obs}$, and residuals—are saved per run to enable full audit. The lens list is processed in a deterministic order with explicit logging of any exclusions and of the two quality–control branches (baseline and outlier–culled). While the baseline model uses the spherical SIS linkage of Eq. (4), the pipeline is modular: alternate mass–profile mappings or dispersion–aperture conventions can be substituted without changing the cosmology layer (Eqs. (1)–(7)) or the estimator (Eq. (9)).

Scope of this section. The methodology above defines the end–to–end path from observables to cosmological constraints without invoking any statistical results or figures. The subsequent sections specify the adopted parameter ranges in Eq. (8), present the curated lens catalog with measurement uncertainties, and then apply the estimator of Eq. (9) to derive profiled one–parameter curves and joint confidence regions for the flat ΛCDM and flat wCDM frameworks.

3 Data: strong–lensing sample and measurements

To implement the methodology of Section 2 we assembled a homogeneous catalog of ∼85 galaxy–scale lenses drawn from three surveys: the Sloan Lens ACS Survey (SLACS), the Lenses Structure and Dynamics survey (LSD), and the Strong Lensing Legacy Survey (SL2S). Our goal was to build a set in which the four quantities required to evaluate $D_{\rm obs}$ for each system are available with uncertainties: the lens and source redshifts (z_l, z_s), the Einstein radius θ_E, and a spectroscopic stellar velocity dispersion for the lens galaxy.

Sources of systems. SLACS provides the bulk of the sample. It identifies early–type lenses by searching SDSS spectra of massive galaxies for background emission lines at $z_s > z_l$ and then confirming viable candidates with *HST*/ACS imaging; the lens mass distribution is modeled to the imaging to recover θ_E with high precision [e.g. 1, 3]. The LSD survey predates SLACS and supplies a handful of well–studied systems for which both imaging and high–quality central dispersions are available; we include the standard subset (e.g., CFRS03.1077, HST 14176+5226, HST 15433+5352, Q0047−281, MG2016+112). SL2S searches CFHTLS imaging for ring–like features around massive red galaxies using the RingFinder algorithm and follows up candidates with *HST* and spectroscopy; we adopt the lenses compiled in Sonnenfeld et al. [13, 14]. In all three surveys the confirmed lenses are dominated by massive early–type galaxies (ETGs), consistent with the expectation that ETGs contain the majority of stellar mass at low redshift and therefore have the highest lensing cross–section.

What is measured and how. For every system we record (z_l, z_s) from spectroscopy, the Einstein radius θ_E from lens–model fits to high–resolution images, and a one–dimensional stellar velocity dispersion. The Einstein radius is obtained by subtracting the light of the deflector (typically a de Vaucouleurs profile) and fitting a lens mass distribution to reproduce the multiply–imaged arcs/ring; the baseline mass model in the survey pipelines is a singular isothermal ellipsoid (SIE) with an external shear term added when required by the data. Although the internal mass–model details differ slightly across surveys and between ground and space imaging, the Einstein radius is a very robust, directly imaged scale: when an explicit error is not published, we adopt a conservative relative uncertainty of 5%, consistent with the survey teams' estimates.

The spectroscopic dispersion is reported as an aperture value $\sigma_{\rm ap}$ measured within a circular fiber or rectangular slit of angular size $\theta_{\rm ap}$. For SLACS we take $\theta_{\rm ap} = 15$ (SDSS fiber); for SL2S and LSD we infer an effective circular aperture from the reported slit dimensions as in the source papers. When the effective (half–light) radius $\theta_{\rm eff}$ is available, we also compute a standardized central dispersion

$$\sigma_0 \;=\; \sigma_{\rm ap}\left(\frac{\theta_{\rm eff}}{2\,\theta_{\rm ap}}\right)^{0.04}, \tag{9}$$

following the Jørgensen et al. aperture correction. Because the exponent is small, the additional uncertainty from $\theta_{\rm eff}$ is negligible ($< 1\%$) compared to the quoted error on $\sigma_{\rm ap}$. Our baseline analysis uses the standardized value $\sigma = \sigma_0$ when available, otherwise $\sigma = \sigma_{\rm ap}$; in both cases the quoted measurement error is propagated.

Catalog contents and formatting. Table 1 (excerpted in the figure below) lists, for each lens: the identifier, z_l, z_s, $\sigma_{\rm ap} \pm \delta\sigma_{\rm ap}$ ($\mathrm{km\,s^{-1}}$), θ_E (arcsec), survey label (SLACS/LSD/SL2S), the adopted $\theta_{\rm ap}$ (arcsec), the effective radius $\theta_{\rm eff}$ (arcsec) when available, and the standardized dispersion $\sigma_0 \pm \delta\sigma_0$ ($\mathrm{km\,s^{-1}}$). All angles are in arcseconds in the table and converted to radians when used in Eq. (5). Quality flags in the working file indicate any peculiarities (e.g., close environment, obvious satellites, or ambiguous arc morphologies).

Selection and quality control. We retain systems with (i) secure measurements of z_l and z_s; (ii) a published θ_E; (iii) a dispersion with an uncertainty; and (iv) $z_s > z_l$. We remove duplicates and keep a single entry per lens following a deterministic rule (most recent and/or highest–quality reduction). After computing $D_{\rm obs} = (c^2/4\pi)\,\theta_E/\sigma^2$ and its uncertainty, we flag systems with $D_{\rm obs} - \sigma_D > 1$ as inconsistent with single–plane FRW geometry under the spherical baseline (possible multi–plane lensing, strong environment, or measurement issues). The baseline cosmology fits use the full quality–controlled catalog; in robustness checks reported later we repeat fits with the flagged systems removed.

Redshift coverage. The combined catalog provides good leverage on late–time geometry: lenses span $z_l \sim 0.1$–0.8 with medians that reflect survey design (SLACS at lower z_l, SL2S intermediate, LSD higher), while sources typically lie at $z_s \gtrsim 1$–3. This lens–source lever arm places the sensitivity squarely in the regime most informative for the ΛCDM/wCDM expansion histories considered here.

Consistency across surveys. Although SLACS, SL2S, and LSD differ in target selection and instrumentation, the quantities we require are reported in a consistent manner. Einstein radii come from forward modeling of the same observables (arc/ring morphology), and dispersion measurements are homogenized through the aperture correction above. As a result, the derived distance–ratio estimator $D_{\rm obs}$ is directly comparable across the full sample and can be confronted, lens by lens, with the theoretical prediction $D_{\rm th}(z_l, z_s; \Theta)$ of Section 2.

A machine–readable version of the catalog (including all columns shown in Table 1 and the propagated $D_{\rm obs}$ and σ_D) accompanies this work.

Table 1: Dataset used in this work.

Name	z_ℓ	z_s	$\sigma_{\rm ap}$ [km s^{-1}]	_E []	Survey	ap (")	$\theta_{\rm eff}$ [$''$]	[km s^1]
J0330-0020	0.351	1.071	212±21	1.1	SLACS	1.5	1.2	220±22
J0405-0455	0.075	0.81	160±8	0.8	SLACS	1.5	1.36	165±8
J0728+3835	0.206	0.688	214± 11	1.25	SLACS	1.5	1.78	219±11
J0737+3216	0.322	0.581	338± 17	1	SLACS	1.5	2.82	339±17
J0808+4706	0.219	1.025	236± 11	1.23	SLACS	1.5	2.42	238±11
J0822+2652	0.241	0.594	259±15	1.17	SLACS	1.5	1.82	264±15
J0841+3824	0.116	0.657	225±11	1.41	SLACS	1.5	4.21	222±11
J0903+4116	0.43	1.065	223±27	1.29	SLACS	1.5	1.78	228±28
J0912+0029	0.164	0.324	326± 12	1.63	SLACS	1.5	3.87	323±12
J0935-0003	0.348	0.467	396±35	0.87	SLACS	1.5	4.24	391±35
J0936+0913	0.19	0.588	243± 12	1.09	SLACS	1.5	2.11	246±12
J0946+1006	0.222	0.608	263±21	1.38	SLACS	1.5	2.35	266±21
J0956+5100	0.24	0.47	334± 17	1.33	SLACS	1.5	2.19	338±17
J0959+0410	0.126	0.535	197±13	0.99	SLACS	1.5	1.39	203±13
J1016+3859	0.168	0.439	247±13	1.09	SLACS	1.5	1.46	254±13
J1020+1122	0.282	0.553	282± 18	1.2	SLACS	1.5	1.59	289±18
J1023+4230	0.191	0.696	242± 15	1.41	SLACS	1.5	1.77	247±15
J1100+5329	0.317	0.858	187±23	1.52	SLACS	1.5	2.24	189±23
J1106+5228	0.096	0.407	262± 13	1.23	SLACS	1.5	1.68	268±13
J1112+0826	0.273	0.63	320±20	1.49	SLACS	1.5	1.5	329±21
J1134+6027	0.153	0.474	239± 12	1.1	SLACS	1.5	2.02	243±12
J1142+1001	0.222	0.504	221±22	0.98	SLACS	1.5	1.91	225±22
J 1143—0144	0.106	0.402	269± 13	1.68	SLACS	1.5	4.8	264±13
J1153+4612	0.18	0.875	226±15	1.05	SLACS	1.5	1.16	235±16
J 1204+0358	0.164	0.631	267±17	1.31	SLACS	1.5	1.47	275±17
J1205+4910	0.215	0.481	281±14	1.22	SLACS	1.5	2.59	283±14
J1213+6708	0.123	0.64	292±15	1.42	SLACS	1.5	3.23	291±15
J 1218+0830	0.135	0.717	219±11	1.45	SLACS	1.5	3.18	218±11
J 1250+0523	0.232	0.795	252±14	1.13	SLACS	1.5	1.81	257±14
J 1251-0208	0.224	0.784	233±23	0.84	SLACS	1.5	2.61	234±23
J 1330-0148	0.081	0.712	185±9	0.87	SLACS	1.5	0.89	194±9
J1402+6321	0.205	0.481	267±17	1.35	SLACS	1.5	2.7	268±17
J1403+0006	0.189	0.473	213±17	0.83	SLACS	1.5	1.46	219±17
J1416+5136	0.299	0.811	240±25	1.37	SLACS	1.5	1.43	247±26
J1430+4105	0.285	0.575	322±32	1.52	SLACS	1.5	2.55	324±32
J1436-OOOO	0.285	0.805	224±17	1.12	SLACS	1.5	2.24	227±17
J1451-0239	0.125	0.52	223± 14	1.04	SLACS	1.5	2.48	225±14
J1525+3327	0.358	0.717	264±26	1.31	SLACS	1.5	2.9	264±26
J1531-0105	0.16	0.744	279±14	1.71	SLACS	1.5	2.5	281±14
J1538+5817	0.143	0.531	189± 12	1	SLACS	1.5	1.58	194± 12
J1621+3931	0.245	0.602	236±20	1.29	SLACS	1.5	2.14	239±20
J1627-0053	0.208	0.524	290± 14	1.23	SLACS	1.5	1.98	295± 14
J1630+4520	0.248	0.793	276±16	1.78	SLACS	1.5	1.96	281±16
J1636+4707	0.228	0.674	231±15	1.09	SLACS	1.5	1.68	236±15
J2238-0754	0.137	0.713	198±11	1.27	SLACS	1.5	2.33	200± 11
J2300+0022	0.228	0.464	279±17	1.24	SLACS	1.5	1.83	285±17
J2303+1422	0.155	0.517	255±16	1.62	SLACS	1.5	3.28	254± 16
J2321-0939	0.082	0.532	249±8	1.6	SLACS	1.5	4.11	246±8
J2341+OOOO	0.186	0.807	207±13	1.44	SLACS	1.5	3.15	207±13
Q0047-2808	0.485	3.595	229±15	1.34	LSD	1.25	0.82	239± 16
CFRS03-1077	0.938	2.941	251±19	1.24	LSD	1.25	1.6	256±19
HST14176	0.81	3.399	224±15	1.41	LSD	1.25	1.06	232± 16
HST15433	0.497	2.092	116±10	0.36	LSD	1.25	0.41	125±11
MG2016	1.004	3.263	328±32	1.56	LSD	0.65	0.31	347±34
J0212-0555	0.75	2.74	273±22	1.27	SL2S	0.9	1.22	277±22

Name	z_ℓ	z_s	$\sigma_{\rm ap}$ [km s^{-1}]	_E []	Survey	ap (")	$\theta_{\rm eff}$ [$''$]	[km s^1]
J0213-0743	0.717	3.48	293±34	2.39	SL2S	1	1.97	293±34
J0214-0405	0.609	1.88	287±47	1.41	SL2S	1	1.21	293±48
J0217-0513	0.646	1.847	239±27	1.27	SL2S	1.5	0.73	253±29
J0219-0829	0.389	2.15	289±23	1.3	SL2S	1	0.95	298±24
J0223-0534	0.499	1.44	288±28	1.22	SL2S	1	1.31	293±28
J0225-0454	0.238	1.199	234±21	1.76	SL2S	1	2.12	233±21
J0226-0420	0.494	1.232	263±24	1.19	SL2S	1	0.84	272±25
J0232-0408	0.352	2.34	281±26	1.04	SL2S	1	1.14	287±27
J0848-0351	0.682	1.55	197±21	0.85	SL2S	0.9	0.45	208±22
J0849-0412	0.722	1.54	320±24	1.1	SL2S	0.9	0.46	338±25
J0849-0251	0.274	2.09	276±35	1.16	SL2S	0.9	1.34	279±35
J0850-0347	0.337	3.25	290±24	0.93	SL2S	0.7	0.28	309±26
J0855-0147	0.365	3.39	222±25	1.03	SL2S	0.7	0.69	228±26
J0855-0409	0.419	2.95	281±22	1.36	SL2S	0.7	1.13	283±22
J0904-0059	0.611	2.36	183±21	1.4	SL2S	0.9	2	182±21
J0959+0206	0.552	3.35	188±22	0.74	SL2S	0.9	0.46	199±23
J1359+5535	0.783	2.77	228±29	1.14	SL2S	1	1.13	233±30
J1404+5200	0.456	1.59	342±20	2.55	SL2S	1	2.03	342±20
J1405+5243	0.526	3.01	284±21	1.51	SL2S	1	0.83	294±22
J1406+5226	0.716	1.47	253±19	0.94	SL2S	1	0.8	262±20
J1411+5651	0.322	1.42	214±23	0.93	SL2S	1	0.85	221±24
J1420+5258	0.38	0.99	246±23	0.96	SL2S	1	1.11	252±24
J1420+5630	0.483	3.12	228±19	1.4	SL2S	1	1.62	230± 19
J2203+0205	0.4	2.15	213±21	1.95	SL2S	1	0.99	219±22
J2205+0147	0.476	2.53	317±30	1.66	SL2S	0.9	0.66	330±31
J2213-0009	0.338	3.45	165±20	1.07	SL2S	1	0.27	179±22
J2219-0017	0.289	1.02	189±20	0.52	SL2S	0.7	1.01	191±20
J2220+0106	0.232	1.07	127±15	2.16	SL2S	1	0.8	132±16
J2221+0115	0.325	2.35	222±23	1.4	SL2S	1	1.12	227±24
J2222+0012	0.436	1.36	221±22	1.44	SL2S	1	1.56	223±22

4 Results

Redshift dependence: D_{ls}/D_s vs z_l

- Per-lens observable: $D_{\rm obs} = \dfrac{c^2}{4\pi}\,\dfrac{\theta_E}{\sigma^2}$ plotted against lens redshift z_l.
- Error bars from quadratic propagation in θ_E and σ; any points with $D_{\rm obs} - \sigma_D > 1$ indicate tension with single-plane FRW under the spherical baseline.

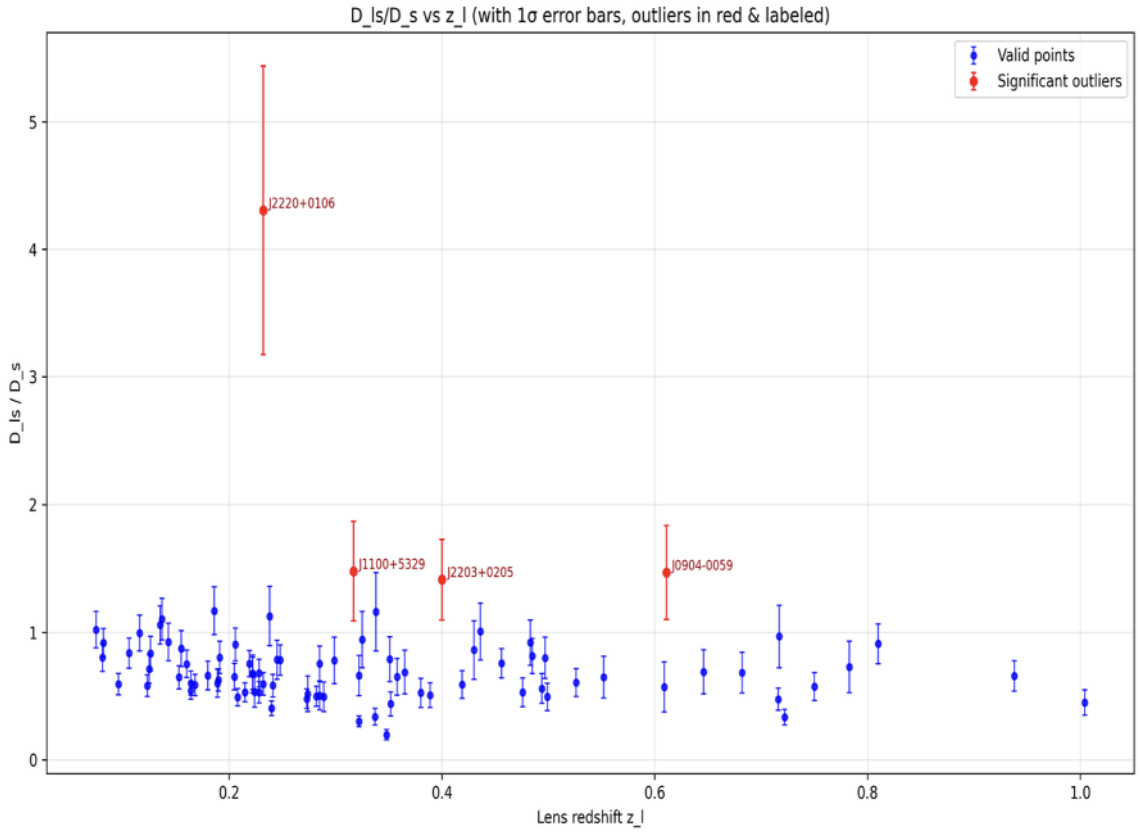

Flat ΛCDM: $\Delta\chi^2$ vs Ω_{m0}

- Profiled curve $\Delta\chi^2(\Omega_{m0}) \equiv \chi^2(\Omega_{m0}) - \chi^2_{\rm min}$ (one parameter).
- Vertical dashed line: best-fit Ω_{m0}; dotted line: $\Delta\chi^2 = 1$ (68% C.L.).

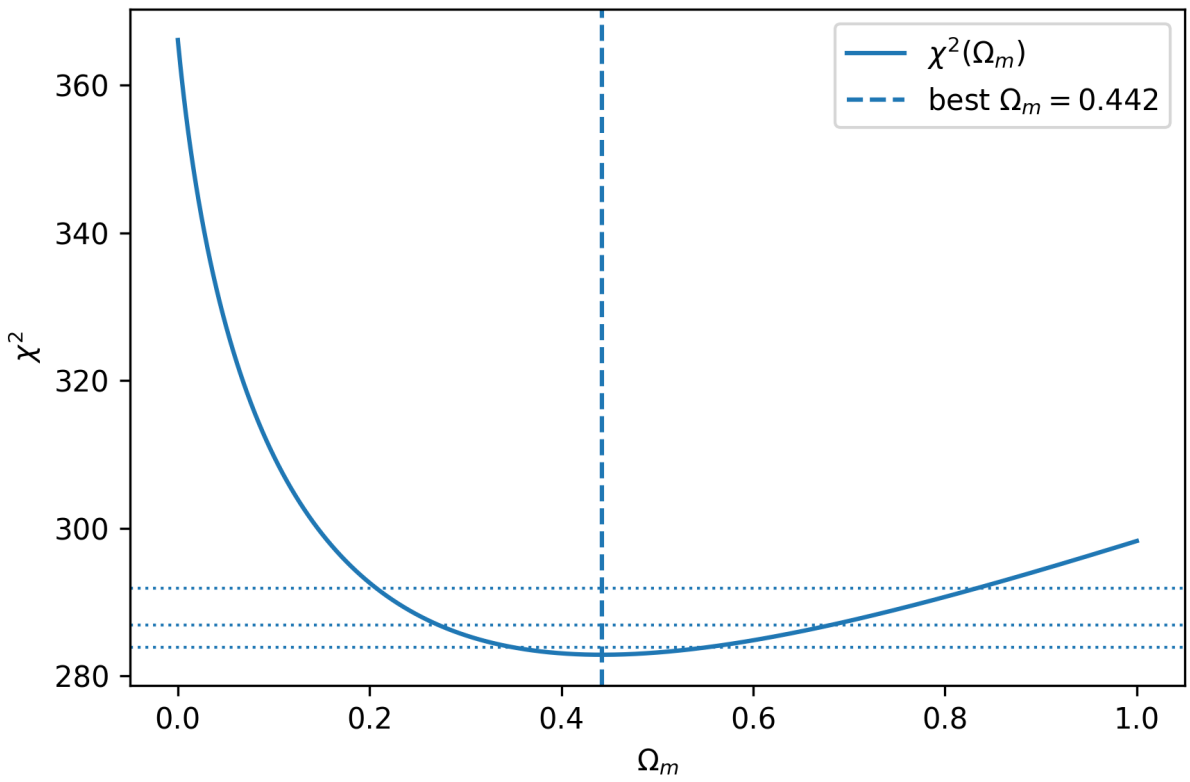

Flat wCDM: $\Delta\chi^2$ vs Ω_{m0} (profiled over w)

- $\Delta\chi^2(\Omega_{m0}) \equiv \min_w \chi^2(\Omega_{m0}, w) - \chi^2_{\min}$.
- Vertical dashed line: best-fit Ω_{m0}; dotted line: $\Delta\chi^2 = 1$.

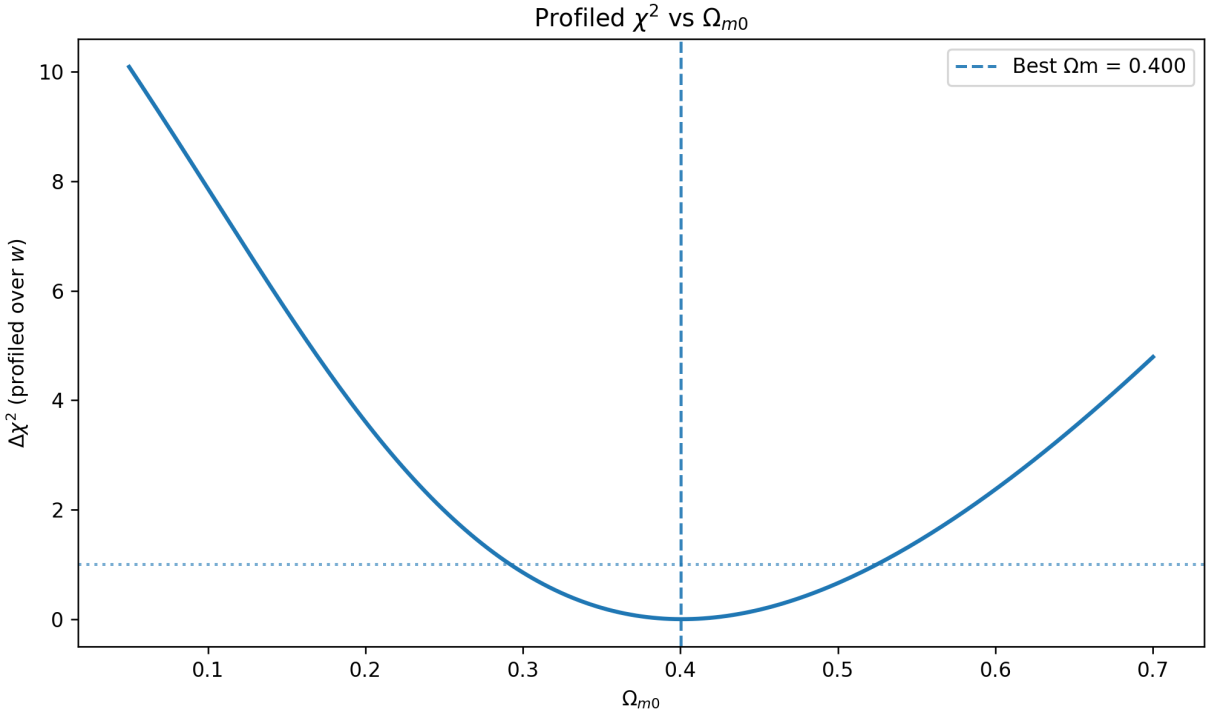

Flat wCDM: $\Delta\chi^2$ vs w (profiled over Ω_{m0})

- $\Delta\chi^2(w) \equiv \min_{\Omega_{m0}} \chi^2(\Omega_{m0}, w) - \chi^2_{\min}$.
- Vertical dashed line: best-fit w; dotted line: $\Delta\chi^2 = 1$.

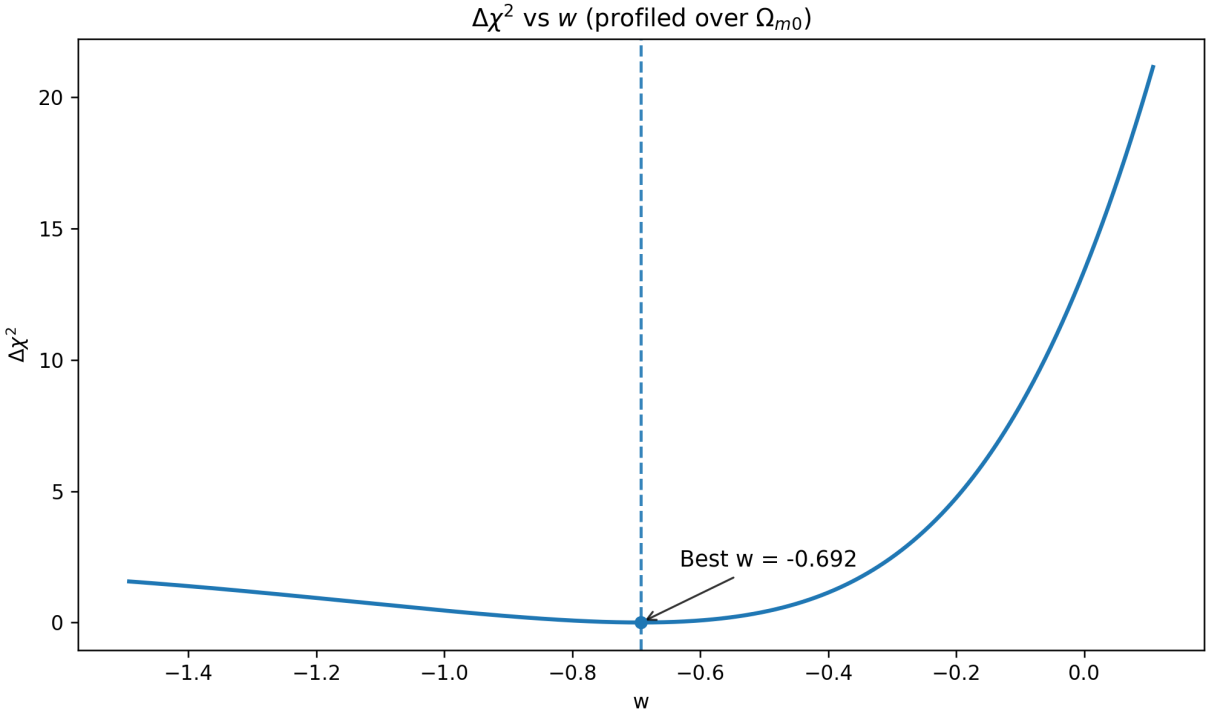

Flat wCDM: joint constraints in $(\Omega_{m0},\, w)$

- Two-parameter confidence regions: $\Delta\chi^2 = \{2.30,\, 6.18,\, 11.83\} \Rightarrow 1\sigma, 2\sigma, 3\sigma$.
- Marker shows the global minimum (best fit).

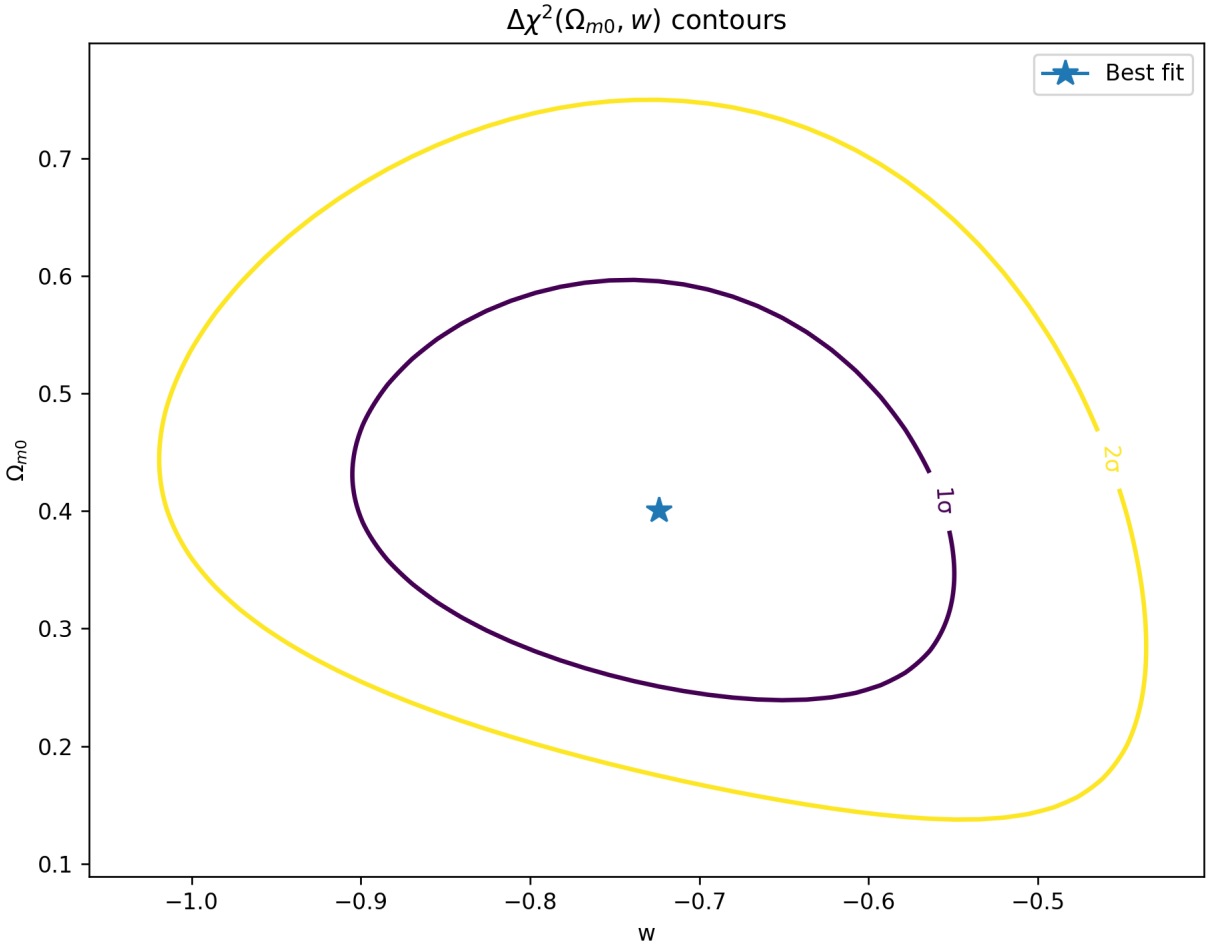

5 Conclusion

We have carried out an end–to–end, lensing–only determination of late–time cosmology using a uniform catalog of ∼85 galaxy–scale strong lenses. The key observable in our analysis is the geometric distance ratio D_{ls}/D_s, inferred for each system from the circularized Einstein radius and an aperture–corrected stellar velocity dispersion. Because the prediction depends only on ratios of angular–diameter distances, the overall H_0 scale cancels, yielding a clean, geometry–based test of the expansion history.

Within flat ΛCDM, profiling the likelihood over a one–dimensional grid produces a clear minimum that favors a present–day matter density of $\Omega_{m0} = 0.442$ with 68% interval $[0.350,\, 0.551]$ and 95% interval $[0.272,\, 0.680]$, from a goodness of fit $\chi^2_{\rm min} \approx 282.864$ for $\nu = 84$ (reduced $\chi^2 \approx 3.37$). These results demonstrate that strong lensing alone selects a well–defined matter density using only geometric information, independent of an external absolute distance calibration.

We then extended the analysis to flat wCDM with a constant dark–energy equation of state. The joint fit yields $(\Omega_{m0},\, w) = (0.400,\, -0.692)$ with $\chi^2_{\rm min} \approx 284.098$ for $\nu = 83$ (reduced $\chi^2 \approx 3.423$). The one–parameter profiles and the two–parameter contours exhibit the expected anti–correlation between Ω_{m0} and w: more negative w pairs with slightly higher Ω_{m0} to keep the distance ratios fixed across the observed lens–source

lever arm. Together with the redshift trend in D_{ls}/D_s versus z_l—which follows the monotonic behavior set by the line–of–sight path lengths—these patterns offer a coherent, physically transparent picture of the constraints provided by the present sample.

Beyond the numerical values, the methodological contribution is a transparent and reproducible pipeline: circularized θ_E from image modeling, standardized dispersions with a mild aperture correction, stable numerical evaluation of the distance integrals, and a simple χ^2 construction that treats every lens in the same way. This modular design is a practical strength. Alternative lens mappings (e.g., power–law slopes), spatial curvature, or a time–varying w can be introduced with minimal changes to the data vector or estimator, and the framework can be combined seamlessly with complementary probes (supernovae, BAO, CMB) for cross–validation or joint inference. As samples grow and measurements sharpen, the approach developed here provides a useful stepping stone: a clean, H_0–independent geometric pipeline that already yields informative late–time constraints and is ready to accommodate richer models and larger data sets.

References

[1] Auger, M. W., Treu, T., Bolton, A. S., et al. (2009). The Sloan Lens ACS Survey. IX. Colors, Lensing, and Stellar Masses of Early-Type Galaxies. *The Astrophysical Journal*, **705**(2), 1099–1115. https://doi.org/10.1088/0004-637X/705/2/1099.

[2] Begeman, K. G. (1989). H I rotation curves of spiral galaxies. I. NGC 3198. *Astronomy & Astrophysics*, **223**, 47–60. ADS link.

[3] Bolton, A. S., Burles, S., Koopmans, L. V. E., et al. (2008). The Sloan Lens ACS Survey. V. The Full ACS Strong-Lens Sample. *The Astrophysical Journal*, **682**(2), 964–984. https://doi.org/10.1086/589327.

[4] Gavazzi, R., Treu, T., Marshall, P. J., et al. (2014). The SL2S Galaxy-Scale Lens Sample. IV. The Dependence of the Total Mass Density Profile of Early-Type Galaxies on Redshift, Stellar Mass, and Size. *The Astrophysical Journal*, **785**, 144. https://doi.org/10.1088/0004-637X/785/2/144.

[5] Jørgensen, I., Franx, M., & Kjærgaard, P. (1995a). Multicolour CCD surface photometry for E and S0 galaxies in 10 clusters. *Monthly Notices of the Royal Astronomical Society*, **273**(4), 1097–1128. https://doi.org/10.1093/mnras/273.4.1097.

[6] Jørgensen, I., Franx, M., & Kjærgaard, P. (1995b). Spectroscopy for E and S0 galaxies in nine clusters. *Monthly Notices of the Royal Astronomical Society*, **276**(4), 1341–1364. https://doi.org/10.1093/mnras/276.4.1341.

[7] Koopmans, L. V. E., Treu, T., Bolton, A. S., Burles, S., & Moustakas, L. A. (2006). The Sloan Lens ACS Survey. III. The Structure and Formation of Early-Type Galaxies and Their Evolution since $z \sim 1$. *The Astrophysical Journal*, **649**(2), 599–615. https://doi.org/10.1086/505696.

[8] Koopmans, L. V. E., Bolton, A. S., Treu, T., et al. (2009). The Structure and Formation of Early-Type Galaxies. *The Astrophysical Journal Letters*, **703**(1), L51–L54. https://doi.org/10.1088/0004-637X/703/1/L51.

[9] Perlmutter, S., Aldering, G., Goldhaber, G., et al. (1999). Measurements of Ω and Λ from 42 High-Redshift Supernovae. *The Astrophysical Journal*, **517**(2), 565–586. https://doi.org/10.1086/307221.

[10] Refsdal, S. (1964). On the Possibility of Determining Hubble's Parameter and the Masses of Galaxies from the Gravitational Lens Effect. *Monthly Notices of the Royal Astronomical Society*, **128**(4), 307–310. https://doi.org/10.1093/mnras/128.4.307.

[11] Riess, A. G., Filippenko, A. V., Challis, P., et al. (1998). Observational Evidence from Supernovae for an Accelerating Universe and a Cosmological Constant. *The Astronomical Journal*, **116**(3), 1009–1038. https://doi.org/10.1086/300499.

[12] Schneider, P., Ehlers, J., & Falco, E. E. (1992). *Gravitational Lenses*. Berlin: Springer. https://doi.org/10.1007/978-1-4612-2756-4.

[13] Sonnenfeld, A., Treu, T., Gavazzi, R., et al. (2013a). The SL2S Galaxy-Scale Lens Sample. I. The Alignment of Mass and Light in Massive Early-Type Galaxies. *The Astrophysical Journal*, **777**(2), 97. https://doi.org/10.1088/0004-637X/777/2/97.

[14] Sonnenfeld, A., Treu, T., Gavazzi, R., et al. (2013b). The SL2S Galaxy-Scale Lens Sample. II. The Inner Density Profiles of Early-Type Galaxies. *The Astrophysical Journal*, **777**(2), 98. https://doi.org/10.1088/0004-637X/777/2/98.

[15] Suyu, S. H., Marshall, P. J., Auger, M. W., et al. (2010). Dissecting the Gravitational Lens B1608+656. II. Precision Measurements of the Hubble Constant, Spatial Curvature, and the Dark Energy Equation of State. *The Astrophysical Journal*, **711**(1), 201–221. https://doi.org/10.1088/0004-637X/711/1/201.

[16] Treu, T., & Koopmans, L. V. E. (2002). The Internal Structure and Formation of Early-Type Galaxies: The Gravitational Lens System MG 2016+112 at $z = 1.004$. *The Astrophysical Journal*, **575**(1), 87–94. https://doi.org/10.1086/341216.

[17] Treu, T., & Koopmans, L. V. E. (2004). Massive Dark Matter Halos and Evolution of Early-Type Galaxies to $z \sim 1$. *The Astrophysical Journal*, **611**(2), 739–760. https://doi.org/10.1086/422245.

[18] Treu, T., Koopmans, L. V. E., Bolton, A. S., Burles, S., & Moustakas, L. A. (2006). The Sloan Lens ACS Survey. II/III. The Structure and Dynamics of Early-Type Lens Galaxies. *The Astrophysical Journal*, **640**(2), 662–677. https://doi.org/10.1086/500124.